


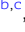
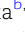

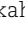










Beyond 2D: A scalable and highly sensitive method for a comprehensive 3D analysis of kidney biopsy tissue

Hiroyuki Yamada ^{a,b,c,d}, Shin-ichi Makino ^{a,b,c}, Issei Okunaga ^a, Takafumi Miyake ^{b,c}, Kanae Yamamoto-Nonaka ^{b,c}, Juan Alejandro Oliva Trejo ^b, Takahiro Tominaga ^a, Maulana A. Empitu ^a, Ika N. Kadariswantiningsih ^a, Aurelien Kerever ^e, Akira Komiya ^f, Tomohiko Ichikawa ^f, Eri Arikawa-Hirasawa ^e, Motoko Yanagita ^{b,c,g} and Katsuhiko Asanuma ^{a,b,c,*}

^aDepartment of Nephrology, Graduate School of Medicine, Chiba University, Chiba 260-8677, Japan

^bThe Laboratory for Kidney Research (TMK Project), Medical Innovation Center, Graduate School of Medicine, Kyoto University, Kyoto 606-8397, Japan

^cDepartment of Nephrology, Graduate School of Medicine, Kyoto University, Kyoto 606-8507, Japan

^dDepartment of Primary Care and Emergency, Graduate School of Medicine, Kyoto University, Kyoto 606-8507, Japan

^eResearch Institute for Diseases of Old Age, Graduate School of Medicine, Juntendo University, Tokyo 113-8421, Japan

^fDepartment of Urology, Graduate School of Medicine, Chiba University, Chiba 260-8677, Japan

^gInstitute for the Advanced Study of Human Biology (ASHBi), Kyoto University, Kyoto 606-8303, Japan

*To whom correspondence should be addressed: Email: kasanuma@chiba-u.jp

Edited By: Dennis Discher

Abstract

The spatial organization of various cell populations is critical for the major physiological and pathological processes in the kidneys. Most evaluation of these processes typically comes from a conventional 2D tissue cross-section, visualizing a limited amount of cell organization. Therefore, the 2D analysis of kidney biopsy introduces selection bias. The 2D analysis potentially omits key pathological findings outside a 1- to 10- μ m thin-sectioned area and lacks information on tissue organization, especially in a particular irregular structure such as crescentic glomeruli. In this study, we introduce an easy-to-use and scalable method for obtaining high-quality images of molecules of interest in a large tissue volume, enabling a comprehensive evaluation of the 3D organization and cellular composition of kidney tissue, especially the glomerular structure. We show that CUBIC and ScaleS clearing protocols could allow a 3D analysis of the kidney tissues in human and animal models of kidney disease. We also demonstrate that the paraffin-embedded human biopsy specimens previously examined via 2D evaluation could be applicable to 3D analysis, showing a potential utilization of this method in kidney biopsy tissue collected in the past. In summary, the 3D analysis of kidney biopsy provides a more comprehensive analysis and a minimized selection bias than 2D tissue analysis. Additionally, this method enables a quantitative evaluation of particular kidney structures and their surrounding tissues, with the potential utilization from basic science investigation to applied diagnostics in nephrology.

Significance Statement

Kidney biopsy has been widely used for diagnosing glomerular kidney diseases. However, it also has a practical problem of not enabling an accurate histopathological diagnosis, such as differentiating focal segmental glomerulosclerosis and crescent glomerulonephritis. This time, we have examined how tissue-clearing techniques resolve the difficulty of kidney histopathological diagnosis through 3D imaging analysis. Our studies reveal that tissue-clearing techniques provide a more comprehensive analysis three-dimensionally and a minimized selection bias compared with that of conventional pathological analysis. Additionally, applying tissue-clearing techniques to used paraffin-embedded human biopsy samples leads to detecting pathological lesions noninvasively with higher sensitivity. These diagnosis platforms could contribute to clinical practice via 3D imaging analysis.

Introduction

A kidney glomerulus is a network of capillaries located at the outer renal cortex. It plays an indispensable role in maintaining homeostasis by producing primitive urine, and prompts the excretion of toxic metabolites and the removal of excess fluids from the body. Meanwhile, the glomerulus retains essential plasma proteins such as albumin and immunoglobulins in the blood through ultrafiltration. A trilaminar structure in the glomerular

capillaries, consisting of glomerular endothelial cells, a glomerular basement membrane (GBM), and podocytes, serves as a filtration barrier to plasma macromolecules. Thus, the glomerulus functions as a molecular sieve to clear the blood and retain necessary elements.

When the glomerulus is damaged by certain factors such as diabetes mellitus, infection, autoantibodies, or drugs, it leads to protein leakage into the urine. More-advanced forms of

Competing Interest: The authors declare no competing interest in this research.

Received: March 3, 2023. **Accepted:** November 6, 2023

© The Author(s) 2024. Published by Oxford University Press on behalf of National Academy of Sciences. This is an Open Access article distributed under the terms of the Creative Commons Attribution-NonCommercial-NoDerivs licence (<https://creativecommons.org/licenses/by-nc-nd/4.0/>), which permits non-commercial reproduction and distribution of the work, in any medium, provided the original work is not altered or transformed in any way, and that the work is properly cited. For commercial re-use, please contact journals.permissions@oup.com

glomerular damage increase the urine protein, which results in kidney failure. Therefore, a kidney biopsy is performed for differential diagnosis of glomerular diseases. Abnormal histopathological findings, such as a crescent formation or extracapillary lesions, could determine the pathological diagnosis of glomerular diseases.

However, problems have plagued the differential diagnoses of glomerular diseases. Particularly, it is occasionally demanding to identify the histopathological abnormalities on an obtained specimen, although these heavily influence the severity classification and diagnosis. One of the reasons for this difficulty is when a biopsy specimen contains an inadequate number of glomeruli. It is sometimes difficult to observe enough glomeruli for histological assessment due to the risk of puncture. Additionally, although an obtained biopsy specimen is a solid body, the portion that is observed is a very thin slice from a cryostat or microtome. That is, the conventional histological assessment two-dimensionally limits the visual field to the cut-slice of biopsy specimens. Therefore, the pathological diagnosis is sometimes inconsistent with the clinical context in some glomerular diseases, such as focal segmental glomerulosclerosis (FSGS) and crescentic glomerulonephritis (1–4).

Tissue-clearing techniques are a chemical process for turning mammalian tissues transparent (5, 6). These techniques enable a 3D visualization of organ structures by allowing the complete penetration of light deep into tissues (7). Several tissue-clearing reagents and protocols have been refined over the past few decades (8, 9). Most of these methods could be less toxic and prevent structural damage, accelerating the progress of 3D imaging for organ structures or even an entire mammalian body (10–13). In fact, tissue-clearing techniques have elucidated numerous molecular mechanisms in kidneys and other organs (14–26).

The contributions that tissue-clearing techniques could make to the clinical treatment of kidneys, however, have remained obscure. Notably, one of the potential advances in tissue-clearing techniques is the enabling of 3D pathological diagnoses, as reported in other organ diagnoses (27–35). Generally, the most common approach for 3D analysis has involved a serial-sectioning method, which is valuable but often labor-intensive, time-consuming, and prone to misinterpretation due to the loss or deformation of sections (12, 36–39). Meanwhile, tissue-clearing techniques smoothly turn an organ transparent so that light can illuminate the tissues in deeper layers. This could expand the coverage of histopathological examination from a thin slice of specimen to an entire unit, potentially contributing to a more accurate clinical diagnosis of glomerular diseases. Thus, we hypothesized that tissue-clearing techniques could have significant potential for improving medical practice.

In the present study, we investigated whether tissue-clearing techniques could be applicable to the pathological diagnosis of human glomerular diseases. We also demonstrated that these techniques could benefit clinical practices in kidney diseases.

Results

ScaleS and CUBIC 3D visualization of the fine structures of glomeruli

First, we aimed to establish which tissue-clearing technique would be the most suitable for the 3D visualization of a glomerulus. As a test model, we used rodent kidneys. Based on the simplicity of the technique and on the applicable chemicals in our country, we selected six optical-clearing protocols: CUBIC, PACT, ScaleS, BABB, iDISCO, and SeeDB2 (40–44). In applying these

protocols, we immunostained with nephrin, which is a marker of kidney glomeruli, and imaged the transparent tissues (Fig. 1A).

Each of these protocols could turn a 1-mm-thick slice of rat kidney transparent (Fig. 1B). This transformation makes it possible to visualize the structure of nephrin-immunostained glomeruli in 3D (Fig. 1C and Videos S1–S7). On the other hand, an entire glomerulus could not be three-dimensionally reconstructed in the non-transparent samples, possibly because of either light reflection or absorption. These results indicated that all these tissue-clearing protocols worked well for the 3D visualization of an entire glomerulus.

Meanwhile, to enable a 3D pathological diagnosis, the ability to visualize the fine glomerular structures is indispensable. Thus, we first examined which clearing protocol could preserve the morphological details of a kidney glomerulus. Using a high-power lens, we magnified the surface of a 3D nephrin-immunostained glomerulus and compared the immunostained morphology. CUBIC and ScaleS protocols clearly showed the meandering structure of nephrin (Fig. 1D and Videos S8–S14). On the other hand, when using BABB, iDISCO, and PACT protocols, we could not visualize the fine structure, possibly because of tissue shrinkage, as the preceding studies mentioned (45). As for the SeeDB2 protocol, although a portion of the slit diaphragm was reconstructed, it was not easy to reconstruct it widely because of fast photobleaching. These results indicated that the CUBIC and ScaleS protocols could be appropriate for the tissue preservation of kidney glomeruli.

Second, to three-dimensionally reconstruct an entire biopsy specimen, the specimen must become transparent enough for lasers to pass through. Thus, using a 1-mm-thick slice of rats' kidneys, we compared the observable depth among CUBIC, ScaleS, and nontransparent samples.

Naturally, in the nontransparent samples, it was impossible to detect the outline of glomeruli at a depth of 100 μm (Fig. 1E and Video S15). Meanwhile, ScaleS made the sample sufficiently transparent to show the entire shapes of glomeruli at a depth of 300 μm (Fig. S1A). Moreover, the CUBIC protocol provided sufficient transparency to visualize the entire 1-mm kidney sample (Fig. 1F and Video S16). Considering that the inner hole of kidney biopsy needles is $\sim 1,000 \mu\text{m}$ (16–18 gauge), the transparency of the CUBIC protocol is sufficient for visualizing an entire biopsy sample.

Collectively, these results indicate that the CUBIC protocol could be applicable to 3D analysis of biopsy tissue in terms of tissue retention and transparency.

3D pathology shows a higher sensitivity in the detection of pathological lesions in glomerular diseases

Based on the above results, we hypothesized that tissue-clearing techniques could contribute to the pathological diagnosis of kidney diseases. To address this question, we generated anti-GBM nephritis rats with clinical severity that reflected the degree of crescent formation, which is an active histological feature of glomerular lesions (Fig. 2A). Then, we compared a conventional 2D diagnosis with our 3D diagnosis using the CUBIC protocol.

Periodic acid-Schiff (PAS) staining revealed crescent formations in several glomeruli of the anti-GBM nephritis group, but such development was undetectable in any of the vehicle group glomeruli (Fig. 2B). Also, immunofluorescence (IF) showed that nephrin was clearly expressed in the glomeruli of the vehicle group. In contrast, in the anti-GBM nephritis group, there was a partial reduction in the expression of nephrin in the glomeruli. Furthermore, the affected lesions exhibited expressions of nuclei and claudin-1,

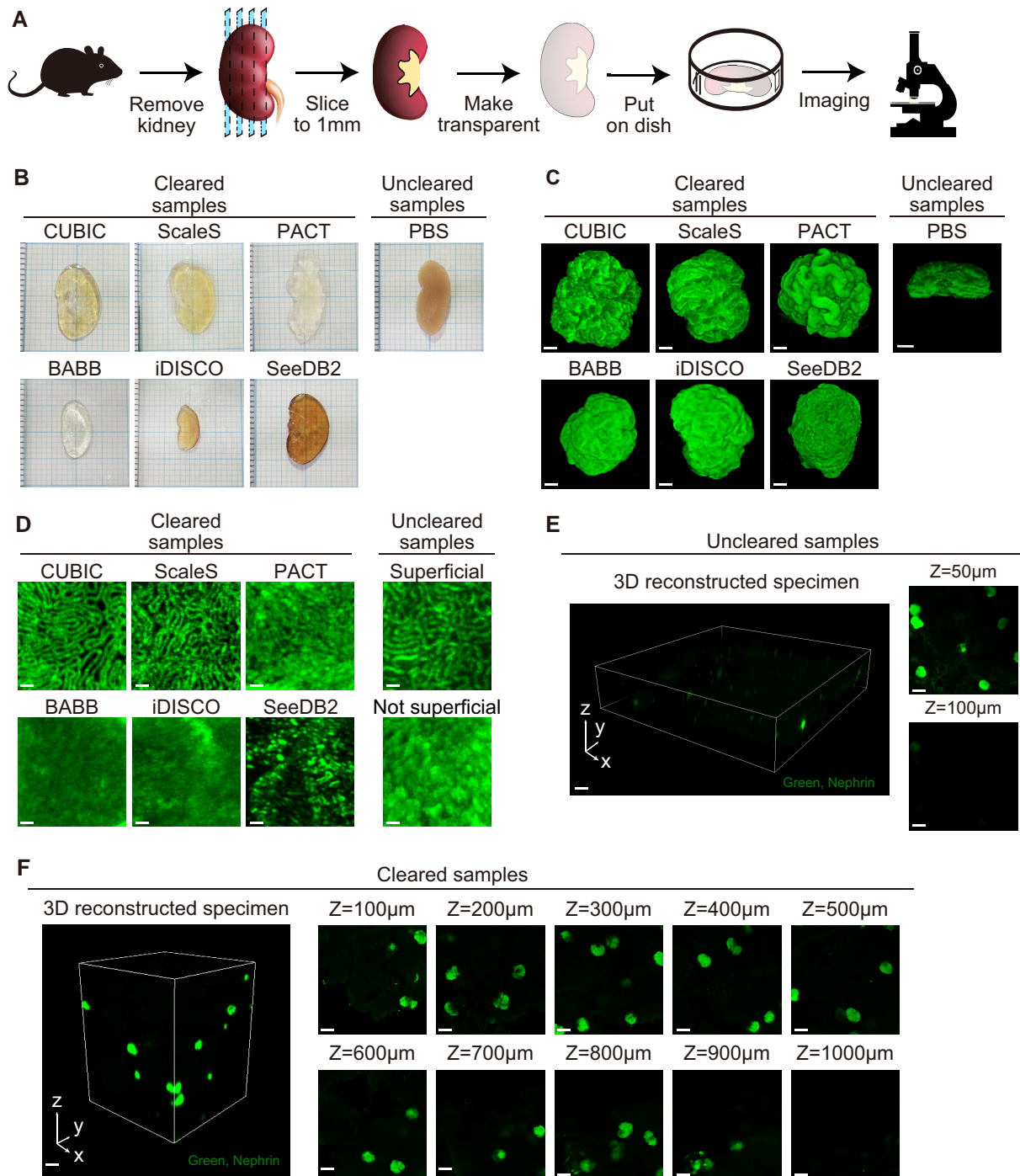


Fig. 1. Evaluation of the suitability of tissue-clearing techniques for observing glomeruli. A) An analysis flow of a rat-dissected kidney with tissue-clearing techniques. B) Visually transparent rat kidney images treated with the respective tissue-clearing techniques. C) Representative images of 3D glomeruli immunostained with nephrin (green), which were treated with each tissue-clearing technique. Bar = 70 and 20 μ m, respectively. D) Representative high-magnification images of 3D glomerulus immunostained with nephrin (green), which were treated with each tissue-clearing technique. Bar = 1 μ m. E) 3D constructed images of a nontransparent rat kidney immunostained with nephrin (green). The right panels show each Z-depth image. Bar = 100 and 150 μ m, respectively. F) 3D constructed images of a transparent rat kidney treated with CUBIC and immunostained with nephrin (green). The right panels show each Z-depth image. Bar = 100 and 150 μ m, respectively.

which is a marker of glomerular parietal epithelial cells (Fig. 2C), indicating the presence of crescent formations. In fact, the crescent formation rate was significantly higher in the anti-GBM nephritis group (14.6 vs. 0.0%, $P < 0.01$; Fig. 2D). These results demonstrated the successful development of the experimental anti-GBM nephritis rats.

Next, we applied the CUBIC protocol to the experimental nephritis rats and analyzed the pathological glomeruli in 3D (Fig. 2E and Video S17). In slice 1, the upper-left portion of the glomerulus showed a claudin-1 expression rather than a nephrin expression, which signaled the existence of a crescent formation. Slice 2 showed similar pathological features in the upper-left portion. However, slice 3 showed the expression of nephrin in the

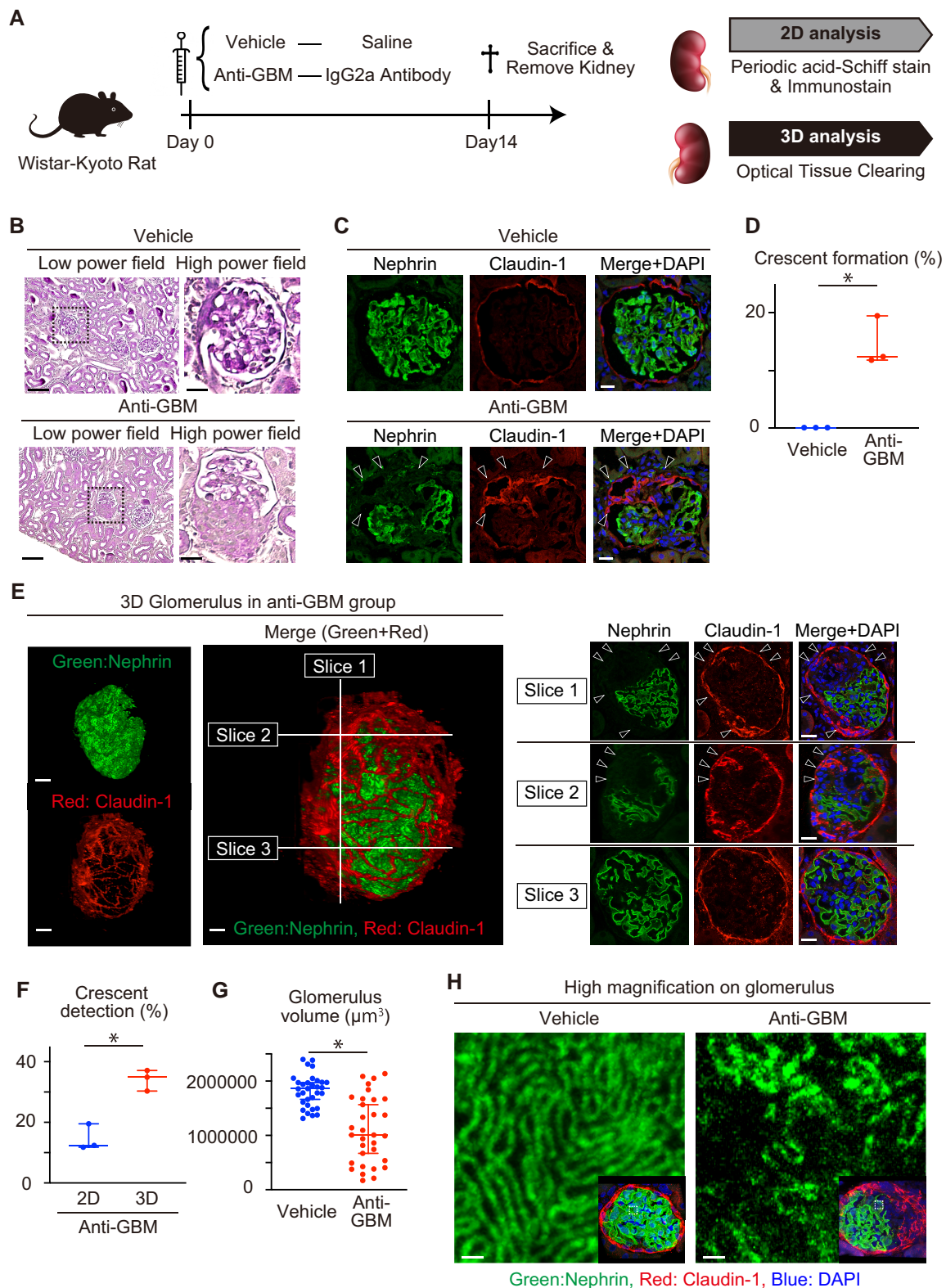


Fig. 2. A 3D pathological examination detects the lesions of glomerular diseases with higher sensitivity. A) An analysis flow of anti-GBM nephritis rats. B) Representative glomerular PAS staining images in the vehicle group and anti-GBM group. Bar = 125 and 20 μm . C) Representative glomerular IF images of nephrin (green), claudin-1 (red), and DAPI (blue) in the vehicle group and anti-GBM group. The arrowheads indicate glomerular pathological lesions of crescent formation. Bar = 20 μm . D) Detection ratio of pathological lesions in the vehicle group and anti-GBM group, using conventional 2D analysis. E) The left panels show 3D overall images of glomeruli in anti-GBM group immunostained with nephrin (green), claudin-1 (red), and DAPI (blue). Bar = 20 μm . The middle panel shows combined images of 3D glomeruli. Bar = 10 μm . The right panels show each slice of glomeruli. Bar = 20 μm . The arrowhead indicates glomerular pathological lesions of crescent formation. F) A comparison of the detection ratio of crescent formation in the anti-GBM group between 2D and 3D analyses. * $P < 0.01$. G) Glomerulus volume in the vehicle group and anti-GBM group. * $P < 0.01$. H) Representative glomerular IF images of nephrin (green) with high magnification in the vehicle group and anti-GBM group. The lower right panel indicates the overall glomerular images immunostained with nephrin (green), claudin-1 (red), and DAPI (blue). Bar = 1 μm .

glomerulus, but not that of claudin-1 despite the same glomerulus. It mistakenly implied an intact staining pattern, although the other slices demonstrated the existence of crescent formations. Meanwhile, any angle observation of vehicle group rats did not reveal a crescent formation (Video S18). These results indicated that 3D analysis enabled the comprehensive workup of the entire glomerulus, although 2D conventional analysis could have caused a false-negative diagnosis.

Based on these results, we broadly analyzed the specimens of both groups of rats using a low-magnification lens. None of the glomeruli in the vehicle group showed glomerulosclerosis (Fig. S1B). Meanwhile, slice 3 in the anti-GBM nephritis group seemed to lack crescent formations in glomeruli “a,” “b,” and “c,” but slice 4 showed that each of them indeed did possess a crescent formation (Fig. S1C).

Quantification of these observable glomeruli in both groups revealed that 3D analysis could detect crescent formations with a significantly higher level of accuracy than conventional 2D analysis (34.1 vs. 14.6%, $P < 0.01$; Fig. 2F). Also, the glomerular volume was significantly smaller in the anti-GBM nephritis group (Fig. 2G).

On the other hand, our previous experiments revealed that the CUBIC protocol has a high capacity for tissue retention. Thus, using a high-magnification lens allowed us to compare the fine structures of glomeruli among both groups (Fig. 2H). The vehicle group preserved the meandering pattern of nephrin. However, such a pattern was not observed in the crescent formation of the anti-GBM nephritis group, and nephrin staining was only partially detected.

These rodent experiments showed that 3D pathological analysis helps prevent a false-negative diagnosis and more accurately identifies lesions, compared with the use of 2D analysis. These results also supported our hypothesis that tissue-clearing techniques are advantageous for the pathological diagnosis of kidney diseases.

Human kidney samples could be analyzed in 3D via the use of tissue-clearing techniques

To apply tissue-clearing techniques to human pathological analysis, it was mandatory to establish whether the CUBIC protocol could render human kidneys transparent. Although Tainaka et al. (40) have already proved that the CUBIC protocol made cadaver kidneys transparent, it remains uncertain whether the CUBIC protocol could enable the 3D pathological analysis of human kidney samples, as it does with rodent samples. Also, it was necessary to establish how transparent and non-destructive the CUBIC protocols could be for human glomerular tissue.

To clarify this, we applied CUBIC delipidating cocktails to the optimal cutting temperature (OCT) compound samples from a kidney that had been removed due to renal cell carcinoma (Fig. 3A). That is, we aimed to identify which delipidating cocktails—CUBIC-1, CUBIC-L, or CUBIC-HL—would be optimal for human kidney tissue. Unfortunately, CUBIC-HL, the most potent lipid eliminator, dematerialized and dissolved the human kidney tissue, possibly due to excessive removal of lipids. The remaining two delipidating cocktails, CUBIC-L and CUBIC-1, rendered the kidney tissues transparent (Fig. S2A).

Next, using glomerulus immunostaining, we examined the optimal combination of these delipidation cocktails and the refractive index (RI)-matching cocktails: CUBIC-2 and CUBIC-R. The combination of CUBIC-R and CUBIC-L outlined the immunostained glomeruli at any depth of the 1 mm specimen (Fig. 3B and

Video S19). Meanwhile, other combinations could not visualize the immunostained glomerulus beyond a depth of 700 μm , possibly due to insufficient lipid removal or RI matching (Fig. S3A–C). When ScaleS was applied, we could not visualize the human samples at a depth similar to that of the rodent samples (Fig. S3D). These results revealed that the combination of CUBIC-L and CUBIC-R enables immunostaining and transparency sufficient for the 3D pathological analysis of human OCT compound kidney samples.

Next, using the transparent human tissue immunostained with nephrin and claudin-1, we reconstructed 3D images of the glomeruli (Fig. 3C and Video S20). The 3D images of both nephrin and claudin-1 were clearly illustrated in a manner similarly to that used with the rodents' samples. Moreover, a high magnification of the nephrin-immunostained glomerulus also showed that the meandering pattern of the nephrin was evidently preserved (Fig. 3D and Video S21).

These results revealed that the CUBIC protocol, CUBIC-L and CUBIC-R, was applicable for 3D pathological analysis of human kidney tissues in terms of transparency, immunostaining, and tissue retention.

Paraffin-embedded kidney samples could be analyzed in 3D through tissue-clearing techniques

Although our above experiments raised the possibility of applying tissue-clearing techniques to 3D pathological analysis, some issues remained. One unresolved issue was how these techniques would be applied to biopsy specimens. The gathering of more biopsy specimens generally translates to a greater chance for an accurate pathological diagnosis. However, more biopsy punctures increase the risk of complications. Particularly in cases of high-risk patients such as those of advanced age or those with coagulopathy, it is neither preferable nor feasible to obtain more specimens only for optical-clearing techniques.

To resolve the above issue, we aimed to develop a platform for the postanalysis of previously analyzed tissues via the use of tissue-clearing techniques. In other words, we planned to recycle biopsy samples. Generally, after the puncture of the kidney biopsy, the obtained tissues are dissected into three segments depending on the purpose: fluorescence immunostaining, electron microscopy, and light microscopy. Most biopsy samples are allocated to light microscopy analysis and are paraffin-embedded for storage. If the paraffin-embedded biopsy samples could be made transparent using tissue-clearing techniques, we could analyze them three-dimensionally without the need for further invasive biopsy punctures.

First, we worked with paraffin-embedded samples of mice before using human paraffin-embedding tissues. That is, we sliced mice paraffin-embedded kidney samples into 1-mm slices similar to human kidney biopsy samples, removed the paraffin, and attempted to make the samples transparent using CUBIC cocktails (Fig. S4A). Unfortunately, the mice samples to which CUBIC-1 was administered as a delipidation cocktail did not become transparent, similar to what was observed in the prior studies (Fig. S4B) (30). Meanwhile, other delipidation cocktails such as CUBIC-L and CUBIC-HL made the paraffin-embedded mice kidney visually transparent (Fig. S4B).

Next, we aimed to clarify which of these remaining cocktails were suitable for the 3D pathological analysis of paraffin-embedded kidney tissues. Thus, we applied these cocktails and nephrin immunostaining to mice paraffin-embedded kidneys

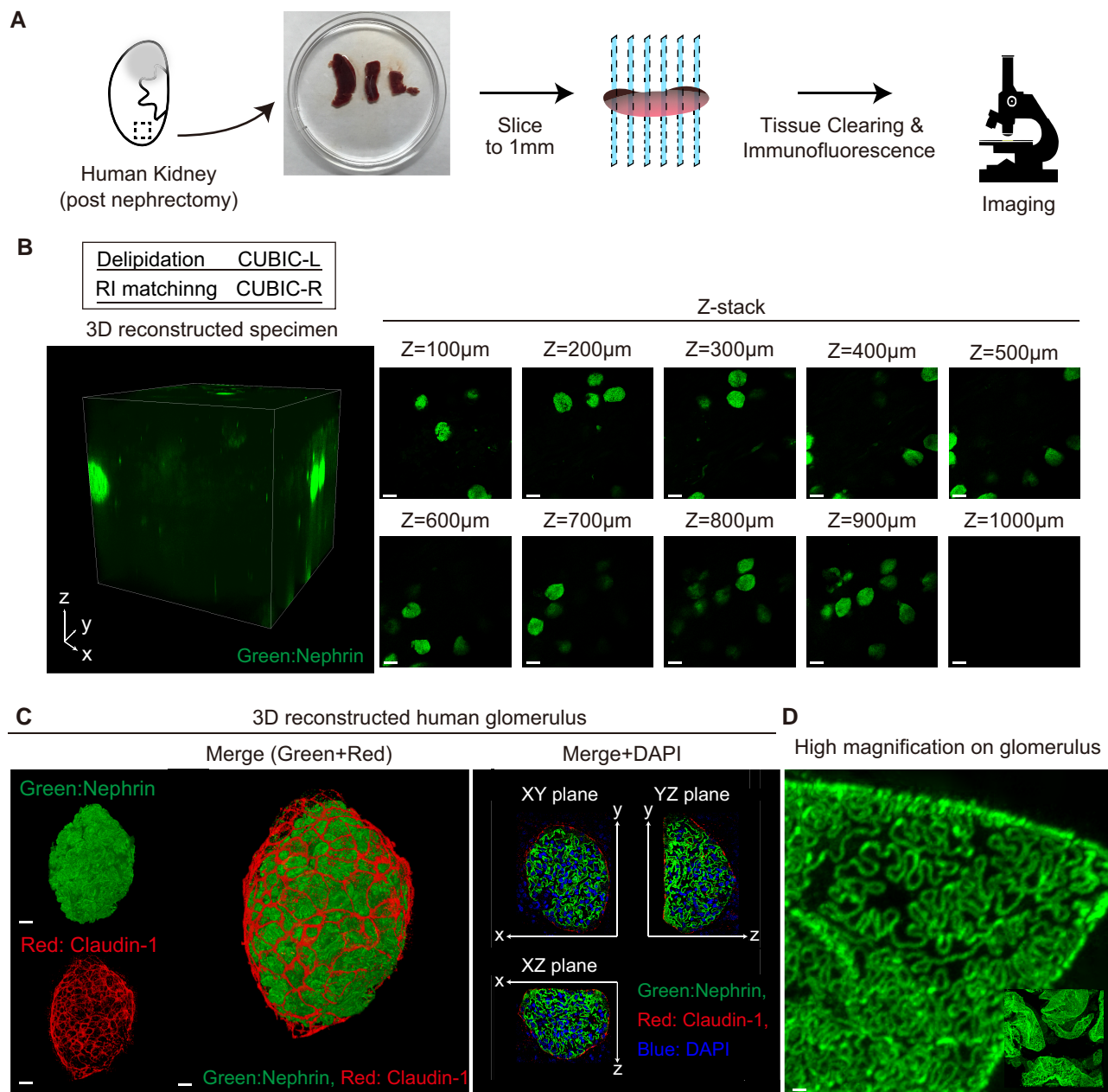


Fig. 3. Human kidney samples could be three-dimensionally analyzed through tissue-clearing techniques. A) An analysis flow of a human-removed kidney with tissue-clearing techniques. B) The left panels show 3D images of a 1-mm-sliced human kidney sample treated with CUBIC-L&R and immunostained with nephrin (green). Bar = μm . The right panel shows each Z-stack image. Bar = $150\ \mu\text{m}$. C) The left panels show 3D overall images of human glomeruli immunostained with nephrin (green), claudin-1 (red), and DAPI (blue). Bar = $20\ \mu\text{m}$. The right panel shows each plane of 3D-immunostained glomerulus. D) Representative high-magnification images of human glomerulus immunostained with nephrin (green). The lower right panel indicates the overall images. Bar = $1\ \mu\text{m}$.

and examined how deeply the IF could be observed in each transparent sample. With CUBIC-2, the deeper layers of the glomeruli could not be visualized, particularly at $>500\ \mu\text{m}$ (Fig. S5A and B). On the other hand, CUBIC-R allowed the observation of nephrin IF at a depth sufficient for the biopsy samples (Fig. S5C and D). Regardless of whether a delipidation cocktail of CUBIC-L or CUBIC-HL was applied, the glomerular immunostaining was not influenced (Fig. S5C and D).

Meanwhile, to recycle the paraffin-embedded kidney tissues to 3D pathological diagnosis with tissue-clearing techniques, it is

crucial to demonstrate that these techniques are nondestructive to glomeruli. That is, we considered it necessary to show that tissue-clearing techniques do not substantially alter the histological structures of glomeruli. To support this hypothesis, we re-embedded the visually transparent mice kidneys in paraffin, which had been treated with CUBIC cocktails, and stained with PAS and hematoxylin–eosin (HE; Fig. S6A). Staining revealed that the glomeruli of posttransparent mice kidneys were nearly identical to the nontissue-clearing samples (Fig. S6B). Tubules and parietal epithelial cells also show no apparent morphological

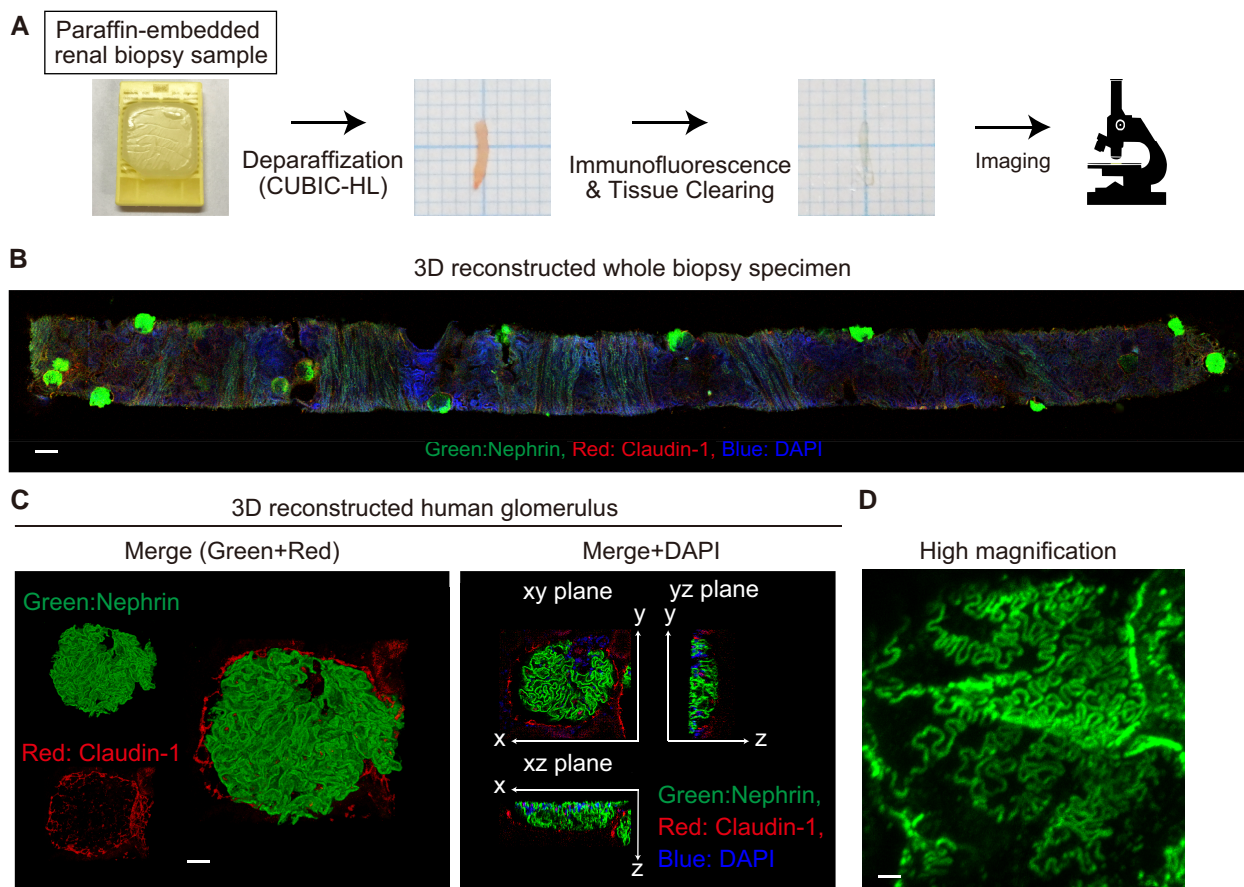


Fig. 4. Paraffin-embedded human kidney samples could be three-dimensionally and noninvasively analyzed through tissue-clearing techniques. A) An analysis flow of a human paraffin-embedded kidney biopsy sample with tissue-clearing techniques. B) A 3D-reconstructed image of the whole human paraffin-embedded kidney biopsy sample immunostained with nephrin (green), claudin-1 (red) and DAPI (blue). Bar = 200 μm . C) A 3D-reconstructed glomerulus of a human paraffin-embedded kidney biopsy sample immunostained with nephrin (green), claudin-1 (red), and DAPI (blue). Bar = 20 μm . D) Representative high-magnification images of human glomerulus on a paraffin-embedded biopsy sample immunostained with nephrin (green). Bar = 1 μm .

alteration among these samples. These findings strongly suggested that CUBIC cocktails have no significant impact on the histopathological diagnosis of kidney diseases.

Recycling of paraffin-embedded human kidney biopsy samples with tissue-clearing techniques noninvasively could analyze the kidney tissue in 3D

Based on the above results of mice paraffin-embedded tissues, we applied the CUBIC-L, CUBIC-HL, and CUBIC-R cocktails to human paraffin-embedded biopsy samples (Fig. 4A). The combination of CUBIC-R and either the delipidation cocktail of CUBIC-L or CUBIC-HL could make the paraffin-embedded biopsy samples transparent (Figs. 4A and S7A). Also, these combinations clearly maintained the nephrin immunostaining (Fig. S7B). However, the claudin-1 immunostaining could not be visualized with CUBIC-L, possibly due to insufficient delipidation, although the nephrin IF was clearly visible (Fig. S7B).

Meanwhile, CUBIC-HL allowed a visualization of the 3D structures of biopsy specimens immunostained with claudin-1 similar to that of nephrin (Fig. 4B and C, and Videos S22 and S23). CUBIC-HL also allowed the visualization of the 3D structures of other molecules, such as laminin and α -smooth-muscle actin, although not-immunostained with the use of CUBIC-L (Fig. S7C). The meandering pattern of nephrin was also sustained, similar

to that in OCT compound samples (Fig. 4D and Video S24). Additionally, even paraffin-embedded specimens stored at room temperature for >10 years were made transparent and showed the 3D glomeruli and meandering pattern of nephrin (Fig. S7D). These results indicated that even in the case of paraffin-embedded human kidney biopsies, tissue-clearing techniques could visualize an entire 3D biopsy specimen and noninvasively enable the 3D pathological analysis of glomeruli.

3D pathology bridges the gap between clinical practice and pathological diagnosis

Using these protocols, we three-dimensionally analyzed the biopsy sample of a rapidly progressive glomerulonephritis (RPGN) case (Table S1). It successfully visualized the 3D image of the whole biopsy specimen (Fig. 5A and Video S25). Next, we observed each 3D visualized glomeruli and analyzed for the pathological glomerulus (Fig. 5B and Video S26). Slice 1 appeared to show like a normal glomerulus. However, in reality, slice 2 revealed the crescent formation despite being from the same glomerulus. That is, these results have demonstrated that 2D conventional analysis presents the serious possibility of a false-negative diagnosis, as our GBM nephritis rats experiments showed.

Next, we analyzed another case of a patient with RPGN, accompanied by interstitial pneumonia caused by antineutrophil cytoplasmic antibody (ANCA)-associated vasculitis. His examination

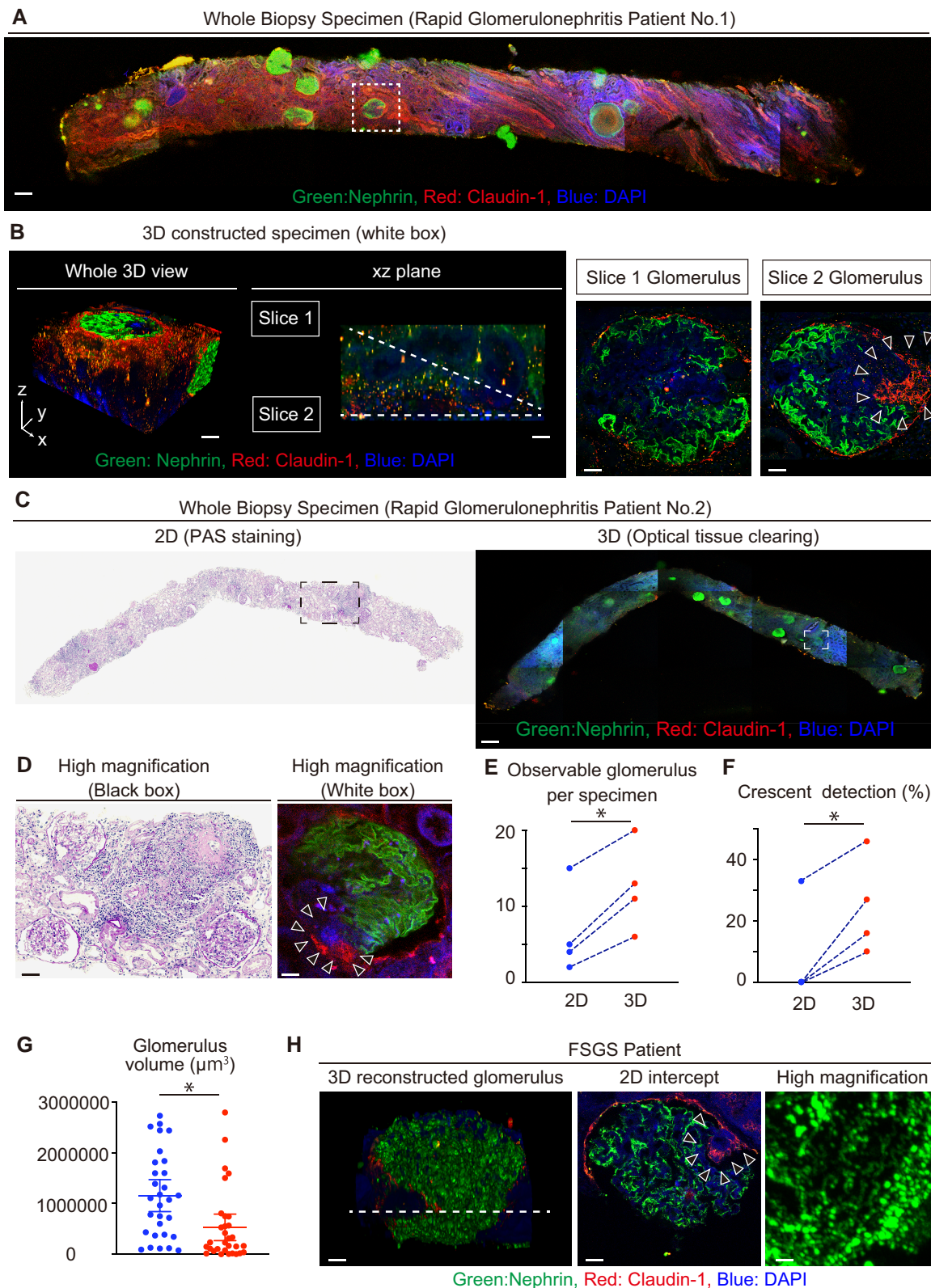


Fig. 5. 3D pathology bridges the gap between clinical practices and pathological diagnosis. A) A whole 3D image of a paraffin-embedded kidney biopsy specimen in RPGN case 1. Bar = 200 μm . B) An analysis of the part of the white-dotted square in A). The left panel shows a 3D-constructed specimen of the white-dotted square. The right panel shows two slices of the 3D-constructed specimen. The arrowheads indicate glomerular pathological lesions of crescent formation. Bar = 20 μm . C) A comparison of the 2D PAS staining with the 3D-constructed specimen in RPGN case 2. The left panel indicates 2D PAS staining, while the right panel indicates a 3D-constructed image. Bar = 200 μm . D) The arrowheads indicate glomerular pathological lesions of crescent formation. Bar = 10 and 20 μm . E) A comparison of a conventional 2D examination with a 3D examination in the observable glomeruli per specimen of RPGN cases. * $P < 0.01$. F) A comparison of a conventional 2D examination with a 3D examination in the detection ratio of RPGN cases' crescent formation. * $P < 0.01$. G) A comparison of glomerular volume in control and RPGN cases. * $P < 0.01$. H) A 3D-reconstructed glomerulus of an FSGS case. The white-dotted line indicates the 2D intercept of the glomerulus. The arrowheads indicate glomerular pathological lesions of crescent formation. Bar = 20, 20, and 1 μm , respectively.

showed urine protein (1.55 g/gCre), microscopic hematuria (10–20/high-power field), and elevated serum creatinine (1.32 mg/dL). These clinical results were compatible with RPGN due to ANCA-associated vasculitis. Thus, to examine the cause of his kidney failure, he received a kidney biopsy. The conventional pathological examination, such as PAS and HE stainings, showed a focal inflammation in the tubules and interstitium. However, the examination did not demonstrate any acute phase of crescent formation in any of the 13 glomeruli, despite it being a typical histological finding in this disease (Figs. 5C and S8). Unfortunately, there was a wide discrepancy between clinical diagnosis and histological findings.

To the paraffin-embedded sample in this case, we applied the tissue-clearing technique (the above technique) and analyzed three-dimensionally (Fig. 5C and Video S27). Indeed, most of the observable glomeruli did not have a crescent formation even though analyzed three-dimensionally. However, a 3D inspection of an entire glomerulus revealed a crescent formation around the intense leucocyte inflammation (Fig. 5D). The abnormal finding by 3D histological analysis was more consistent with the clinical course. Finally, the patient achieved remission with steroid administration.

Upon further investigation, we quantified a series of RPGN cases. The 3D analysis could observe more glomeruli per biopsy specimen (9.2 vs. 14.4, $P < 0.05$; Fig. 5E). Additionally, as 3D analysis helps prevent a false-negative diagnosis, it also facilitates a more sensitive detection of crescent formation (8.3 vs. 16.5%, $P < 0.05$; Fig. 5F). Moreover, it showed a smaller volume of immunostained glomeruli in patients with RPGN compared with the control group (Fig. 5G). These analyses demonstrated the superiority of 3D analysis over conventional analyses, leading to accurate pathological diagnoses.

The crescent formation is an abnormal finding of not only RPGN but also various glomerulonephritis. The finding is frequently detected in severe glomerulonephritis and is decisive for a differential diagnosis between focal segmental sclerosis and minimal change from nephrotic syndrome. The prognosis of these two diseases is inverted despite similar symptoms and clinical context. Nonetheless, it remains challenging to differentiate the two using current clinical and pathological examination methods.

To address the above difficulty, we applied tissue-clearing techniques to the paraffin-embedded sample of an FSGS case (Fig. 5H and Video S28). The crescent formation of FSGS was also three-dimensionally visualized. Also, the high magnification of 3D-constructed glomeruli did not show the meandering pattern of nephrin. These results indicated that tissue-clearing techniques could be valuable for differentiating various glomerular diseases and evaluating severity.

Discussion

Kidney biopsy is the gold-standard examination for glomerular disease diagnosis. Nonetheless, it has major limitations regarding the accurate identification of histopathological findings. Meanwhile, tissue-clearing techniques smoothly enable the 3D visualization of organ structures, which allows the elucidation of various molecular mechanisms. The present study has demonstrated which tissue-clearing techniques are suitable for 3D pathological analysis of kidney samples and how these techniques could be applied to human kidney biopsy samples (Table S2). These results also show that these techniques could greatly and noninvasively contribute to clinical practice via 3D pathological diagnosis of glomeruli.

Previous studies have also examined the applicability of tissue-clearing techniques to human kidney samples. Unnersjö-Jess et al. (23) demonstrated the simplicity and usefulness of their tissue-clearing protocol on human kidney samples. They also indicated that their clearing protocol is applicable to human paraffin-embedded samples (46). However, their paraffin samples were dissected into 200 μm slices, which is significantly thinner than the standard biopsy sample thickness of 1,000 μm . Additionally, they did not seem to visualize the 3D glomerular images, possibly due to insufficient staining or transparency. Meanwhile, our study could visualize the entire 3D image of the paraffin-embedded human kidney biopsy samples that were about 800 μm in thickness. These results show that 3D pathological diagnosis is applicable to clinical practice.

Tainaka et al. (40) also proved that the CUBIC protocol enables sufficient tissue-clearing and compatibility with immunostaining using human kidney samples. They suggested the use of CUBIC-HL for the delipidation of human kidney samples. On the other hand, we examined the applicability of the CUBIC protocol using two kinds of human kidney samples: OCT compound samples and paraffin-embedded samples.

In contrast to their study results, our results show that CUBIC-L, a milder delipidation cocktail, is even better for the delipidation of OCT compound samples, while CUBIC-HL is the most refined delipidation cocktail of paraffin-embedding kidney samples (Fig. S9). We realized that the reason for these differences lies in the lipid content of the two embedding medium: OCT compound and paraffin. As paraffin is an alkaline wax substance with hydrating properties, stronger delipidation could be appropriate for adequate tissue clearing and IF. Meanwhile, for OCT compound kidney samples, milder delipidation could be more suitable because the OCT compound is a formulation of clear, water-soluble glycols and resins.

Additionally, our results indicated that the 3D pathological analysis shows higher sensitivity for crescent formation than the 2D analysis. Because 3D analysis enables a comprehensive visualization of the tissue specimens from every angle, it could prevent a false-negative diagnosis of pathological lesions. In other words, tissue-clearing techniques enable an accurate differential diagnosis of glomeruli. This could resolve the possible discrepancy between clinical context and histopathological findings in glomerular disease diagnoses.

Our study has a few limitations. First, we have not examined the adaptability of other tissue-clearing techniques to human biopsy samples based on our rodent test results. Second, our definition of crescent formation in IF staining is not generalized well. Thus, there is a small possibility of some diagnosis discrepancies between conventional 2D staining and 3D immunostaining. Similar definitions have been made, however, in various other immunostaining studies (21, 47, 48). Third, not all the antibodies used for 2D immunostaining are technically applicable to tissue-clearing techniques. Therefore, we could not deny the possibility that other combinations of molecules might be more advantageous than our study using nephrin and claudin-1.

Conclusion

With the use of tissue-clearing techniques, we were able to visualize the 3D fine structure of kidney glomeruli in humans and rodents. The arrangement of tissue-clearing cocktails also enabled the 3D evaluation of an entire human biopsy sample, regardless of the stock medium. Thus, we could detect pathological

lesions with higher sensitivity by making a comparison with the conventional 2D method. Notably, the 3D evaluation of paraffin-embedded tissues could add even more information for diagnosing glomerular diseases—and, importantly, in a non-invasive manner. We anticipate that these techniques could contribute much to the clinical treatment of kidney disease.

Materials and methods

Animal kidney samples

Rats and mice were maintained on 12 h/12 h light/dark cycle with food and water available ad libitum. All animal handling and experiments were performed strictly in accordance with the recommendations of the guidelines laid down by the National Institute for Health Guide for the Care and Use of Laboratory Animals. This experimental protocol was approved by the Animal Research Committee of Kyoto University: (No. Med Kyo 14121) and (No. A30-136). Excised kidneys were fixed with 4% paraformaldehyde (PFA) in phosphate-buffered saline (PBS) at 4°C overnight (49).

Tissue-clearing techniques for OCT compound samples

To remove PFA and for the following cryopreservation, the fixed samples were immersed in 20% sucrose PBS solution at 4°C overnight. These samples were cut into 1-mm slices using a brain slicer (Muromachi Kikai, Tokyo, Japan). If necessary, the sample was stocked in OCT compound (Sakura Finetek, Tokyo, Japan) at -80°C until use. When the frozen sample was applied to clearing protocols, it was thawed and vigorously washed with PBS before use.

The procedures of optical tissue clearing for rat kidney samples were performed using a 24-well dish as reported in each clearing protocol (41–44, 50, 51). For human kidney samples, this study applied ScaleS and CUBIC as a means to analyze the kidney in 3Ds. The ScaleS protocol was also used for human kidney samples, following the original protocol. Meanwhile, in the CUBIC protocol, the delipidation cocktail employed CUBIC-L instead of CUBIC-HL, unlike the original protocol.

Immunostaining during tissue-clearing techniques

The whole process of immunostaining was performed using a 24-well dish. Before starting the immunostaining, to prevent contamination, the samples were washed gently and thoroughly with the antibody dilution solution that was stipulated by each protocol (41–44, 50, 51). The samples were immersed in the primary antibody solution (750–1,000 μ L) on a horizontal shaker at room temperature for two overnights. Then, the samples were washed with the antibody dilution solution of each tissue-clearing protocol for 30 min \times 3. The secondary antibody solution (750–1,000 μ L) was added to the sample on a horizontal shaker at room temperature for two overnights. The order of tissue clearing and IF followed each protocol's recommendations.

The primary antibodies used in this study were goat antimouse nephrin antibody (AF3159; R & D Systems, Minneapolis, MN, USA), sheep antihuman nephrin antibody (AF4269; R & D Systems), and rabbit anti-claudin-1 antibody (ab15098; Abcam, Cambridge, MA, USA). The secondary antibodies were Alexa Fluor-488 antgoat IgG antibody (Thermo Fisher Scientific, Waltham, MA, USA) and Alexa Fluor-555 antirabbit IgG antibody (Thermo Fisher Scientific). The dilution ratios of

the primary and secondary antibodies were 1:100, and 1:300, respectively. DAPI (Roche, Basel, Switzerland) was used for nuclei staining.

Image acquisition and reconstruction

The transparent samples were placed onto a glass bottom dish (Greiner Bio-One, Krems, Austria). To prevent the drying out, a few drops of the final immersed solution of each protocol were also added to the sample on the dish. Images of transparent tissues and stained slides were acquired using a Leica TSC SP8 confocal microscopy system (Leica, Wetzlar, Germany) and a LSM780 (Carl Zeiss, Jena, Germany). The 3D images of the entire 1-mm or biopsy specimen were taken using a 10 \times objective lens. The 3D mouse and human glomeruli images were taken using a 40 \times objective lens. For high-magnification images, such as the nephrin meandering pattern, a 100 \times objective lens was utilized. For image reconstruction, Z-stack projections were performed using ImageJ (ImageProcessing and Analysis in Java; <http://imagej.nih.gov/ij/>); 3D rendering was performed using Imaris 8.1.2 (Bitplane, Zurich, Switzerland).

Anti-GBM nephritis

Anti-GBM nephritis was developed according to a protocol established as reported previously (52). Kidney disease was induced in male Wistar-Kyoto (WKY) rats aged 5 weeks (body weight, 90–120 g) by injection of antirat mAb, a84 (Chondrex, Redmond, WA, USA; 100 mg/kg, intraperitoneally). Rats ($n=3$ per group) were euthanized on day 14 after the injection of antibody or saline, and the kidneys were harvested. Saline-injected age-matched WKY rats ($n=3$) served as controls.

PAS and HE staining

Fixed kidney samples were embedded in paraffin after dehydration as previously described (53). Paraffin blocks were sectioned in 2- μ m thicknesses and stained with PAS and HE for histologic evaluation by light microscopy. The stained slides were observed under a bright field using BZ-X710 (Keyence, Osaka, Japan). After observing all the glomeruli, the ratio of the glomerulus with crescent formation was calculated.

Immunostaining for 2D analysis

Similarly, as stated above, the fixed samples were immersed in 20% sucrose PBS solution and frozen in OCT compound. Double IF and poststaining with DAPI were performed as described previously (54).

Human kidney samples

Human kidney samples were allocated from a part of the excised kidney due to renal cell carcinoma (RCC) in the Department of Urology at Chiba University. Human paraffin biopsy samples were obtained from diagnostic renal biopsies performed in the Department of Nephrology at Chiba University. The study protocol was approved by the ethics committee on human research of the Chiba University Hospital: no. 856(770) and no. 3665. Informed consent was obtained from all participants.

Deparaffinization of tissues from paraffin-embedded blocks

Paraffin-embedded biopsy samples were punched out using a scalpel. The excised samples were washed with Hemo-De (FALMA, Tokyo, Japan) in an Eppendorf tube to remove the

paraffin. The samples were washed for 1 h, overnight, and then 1 h again. Subsequently, the samples were washed with 100, 90, 80, and 70% ethanol-diluted water for 90 min each. After an overnight wash with PBS, the samples were subjected to each tissue-clearing technique.

Tissue-clearing techniques for paraffin-embedded samples

After deparaffinization, the samples were placed in a 24-well dish and fully immersed in CUBIC-HL (750–1,000 μ L) on a horizontal shaker at room temperature for three nights. After a 30-min wash with PBS, followed by an overnight wash and another 30-min wash, the IF procedure was performed as described above. Following three 30-min washes with PBS, the samples were immersed in CUBIC-R on a horizontal shaker overnight at room temperature.

Statistical analysis

All data are expressed as the median and 95% CIs. An unpaired t test was used for the comparison between the two groups. Meanwhile, for the comparison between two observations of the same specimen, a paired t test was used. A P-value <0.05 was considered statistically significant. All statistical data were analyzed using JMP for Macintosh version 10.0.2 software (SAS Institute, Tokyo, Japan).

Acknowledgments

The authors thank Prof. Hiroyuki Hioki (Department of Cell Biology and Neuroscience, Juntendo University Graduate School of Medicine) for his excellent advice. The authors thank Prof. Michiyuki Matsuda and Ms. Kanako Takakura for their technical advice (Live Imaging Center, Kyoto University). They thank Prof. Toshinori Nakayama, Dr Motoko Y. Kimura, and Dr Kiyoshi Hirahara for their equipment support (Department of Immunology, Chiba University). The authors thank Ms Chihiro Nakagawa, Ms Yuri Ogawa, Mrs Chihiro Makino, and Ms Mayu Miyaki for their excellent technical assistance.

Supplementary Material

[Supplementary material](#) is available at PNAS Nexus online.

Funding

This work was supported in part by the Kyoto University Live Imaging Center, Grants-in-Aid KAKENHI 16H06280 “Advanced Bioimaging Support,” and a Ministry of Education, Culture, Sports, Science and Technology of Japan Grant-in-Aid for Scientific Research, 17K19653, 26670431 (to K.A.).

Author Contributions

H.Y. and K.A. designed the research and wrote the manuscript. H.Y., S.M., I.O., T.M., K.Y.-N., J.A.O.T., T.T., M.A.E., and I.N.K. conducted the experiments. A.K. and E.A.H. provided technical support and advice. A.K. and T.I. contributed materials. M.Y. and K.A. supervised the whole project.

Data Availability

All data required to assess the conclusions in this paper are presented in the manuscript, figures, supplementary figures, and

supplementary videos. The dataset for supplementary videos is available on Zenodo (<https://zenodo.org/record/8146215>).

References

- 1 Maas RJ, Deegens JK, Smeets B, Moeller MJ, Wetzels JF. 2016. Minimal change disease and idiopathic FSGS: manifestations of the same disease. *Nat Rev Nephrol.* 12:768–776.
- 2 Stokes MB, Markowitz GS, Lin J, Valeri AM, D’Agati VD. 2004. Glomerular tip lesion: a distinct entity within the minimal change disease/focal segmental glomerulosclerosis spectrum. *Kidney Int.* 65:1690–1702.
- 3 Baldwin DS, Neugarten J, Feiner HD, Gluck M, Spinowitz B. 1987. The existence of a protracted course in crescentic glomerulonephritis. *Kidney Int.* 31:790–794.
- 4 Jindal KK. 1999. Management of idiopathic crescentic and diffuse proliferative glomerulonephritis: evidence-based recommendations. *Kidney Int.* 55:S33–S40.
- 5 Aswendt M, Schwarz M, Abdelmoula WM, Dijkstra J, Dedeurwaerdere S. 2017. Whole-brain microscopy meets in vivo neuroimaging: techniques, benefits, and limitations. *Mol Imaging Biol.* 19:1–9.
- 6 Ueda HR, et al. 2020. Tissue clearing and its applications in neuroscience. *Nat Rev Neurosci.* 21:61–79.
- 7 Yu T, Zhu J, Li D, Zhu D. 2021. Physical and chemical mechanisms of tissue optical clearing. *iScience.* 24:102178.
- 8 Tainaka K, Kuno A, Kubota SI, Murakami T, Ueda HR. 2016. Chemical principles in tissue clearing and staining protocols for whole-body cell profiling. *Annu Rev Cell Dev Biol.* 32:713–741.
- 9 Weiss KR, Voigt FF, Shepherd DP, Huisken J. 2021. Tutorial: practical considerations for tissue clearing and imaging. *Nat Protoc.* 16:2732–2748.
- 10 Richardson DS, Lichtman JW. 2015. Clarifying tissue clearing. *Cell.* 162:246–257.
- 11 Vigouroux RJ, Belle M, Chedotal A. 2017. Neuroscience in the third dimension: shedding new light on the brain with tissue clearing. *Mol Brain.* 10:33.
- 12 Yu T, Qi Y, Gong H, Luo Q, Zhu D. 2017. Optical clearing for multi-scale biological tissues. *J Biophotonics.* 11(2). doi:10.1002/jbio.201700187.
- 13 Susaki EA, Ueda HR. 2016. Whole-body and whole-organ clearing and imaging techniques with single-cell resolution: toward organism-level systems biology in mammals. *Cell Chem Biol.* 23:137–157.
- 14 Puelles VG, Combes AN, Bertram JF. 2021. Clearly imaging and quantifying the kidney in 3D. *Kidney Int.* 100:780–786.
- 15 Puelles VG, et al. 2016. Validation of a three-dimensional method for counting and sizing podocytes in whole glomeruli. *J Am Soc Nephrol.* 27:3093–3104.
- 16 Klingberg A, et al. 2017. Fully automated evaluation of total glomerular number and capillary tuft size in nephritic kidneys using lightsheet microscopy. *J Am Soc Nephrol.* 28:452–459.
- 17 Unnersjö-Jess D, et al. 2018. Confocal super-resolution imaging of the glomerular filtration barrier enabled by tissue expansion. *Kidney Int.* 93:1008–1013.
- 18 Schuh CD, et al. 2018. Combined structural and functional imaging of the kidney reveals major axial differences in proximal tubule endocytosis. *J Am Soc Nephrol.* 29:2696–2712.
- 19 Saritas T, et al. 2018. Optical clearing in the kidney reveals potassium-mediated tubule remodeling. *Cell Rep.* 25:2668–2675.e3.

- 20 Hasegawa S, et al. 2019. Comprehensive three-dimensional analysis (CUBIC-kidney) visualizes abnormal renal sympathetic nerves after ischemia/reperfusion injury. *Kidney Int.* 96:129–138.
- 21 Puelles VG, et al. 2019. Novel 3D analysis using optical tissue clearing documents the evolution of murine rapidly progressive glomerulonephritis. *Kidney Int.* 96:505–516.
- 22 Blanc T, et al. 2021. Three-dimensional architecture of nephrons in the normal and cystic kidney. *Kidney Int.* 99:632–645.
- 23 Unnersjö-Jess D, et al. 2021. A fast and simple clearing and swelling protocol for 3D in-situ imaging of the kidney across scales. *Kidney Int.* 99:1010–1020.
- 24 Liu H, et al. 2021. Heterozygous mutation of *Vegfr3* reduces renal lymphatics without renal dysfunction. *J Am Soc Nephrol.* 32:3099–3113.
- 25 Huang J, et al. 2019. A cationic near infrared fluorescent agent and ethyl-cinnamate tissue clearing protocol for vascular staining and imaging. *Sci Rep.* 9:521–521.
- 26 Motrapu M, et al. 2020. Drug testing for residual progression of diabetic kidney disease in mice beyond therapy with metformin, ramipril, and empagliflozin. *J Am Soc Nephrol.* 31:1729–1745.
- 27 Liu JTC, et al. 2021. Harnessing non-destructive 3D pathology. *Nat Biomed Eng.* 5:203–218.
- 28 Almagro J, Messal HA, Zaw Thin M, van Rheenen J, Behrens A. 2021. Tissue clearing to examine tumour complexity in three dimensions. *Nat Rev Cancer.* 21:718–730.
- 29 Parra-Damas A, Saura CA. 2020. Tissue clearing and expansion methods for imaging brain pathology in neurodegeneration: from circuits to synapses and beyond. *Front Neurosci.* 14:914.
- 30 Nojima S, et al. 2017. CUBIC pathology: three-dimensional imaging for pathological diagnosis. *Sci Rep.* 7:9269.
- 31 Sabyusheva Litschauer I, et al. 2020. 3D histopathology of human tumours by fast clearing and ultramicroscopy. *Sci Rep.* 10:17619.
- 32 Pan C, et al. 2019. Deep learning reveals cancer metastasis and therapeutic antibody targeting in the entire body. *Cell.* 179:1661–1676.e19.
- 33 Gómez-Gaviro MV, Sanderson D, Ripoll J, Desco M. 2020. Biomedical applications of tissue clearing and three-dimensional imaging in health and disease. *iScience.* 23:101432.
- 34 Brenna C, et al. 2022. Optical tissue clearing associated with 3D imaging: application in preclinical and clinical studies. *Histochem Cell Biol.* 157:497–511.
- 35 Lin Y-Y, et al. 2022. Computer-assisted three-dimensional quantitation of programmed death-ligand 1 in non-small cell lung cancer using tissue clearing technology. *J Transl Med.* 20:131–131.
- 36 Deng R, et al. 2022. Dense multi-object 3D glomerular reconstruction and quantification on 2D serial section whole slide images. *Proc SPIE Int Soc Opt Eng.* 12039:120390F.
- 37 Li J, Lin P, Tan Y, Cheng J-X. 2019. Volumetric stimulated Raman scattering imaging of cleared tissues towards three-dimensional chemical histopathology. *Biomed Opt Express.* 10:4329–4339.
- 38 Mikula S, Denk W. 2015. High-resolution whole-brain staining for electron microscopic circuit reconstruction. *Nat Methods.* 12:541–546.
- 39 Svensson RB, et al. 2017. Evidence of structurally continuous collagen fibrils in tendons. *Acta Biomater.* 50:293–301.
- 40 Tainaka K, et al. 2018. Chemical landscape for tissue clearing based on hydrophilic reagents. *Cell Rep.* 24:2196–2210.e9.
- 41 Yang B, et al. 2014. Single-cell phenotyping within transparent intact tissue through whole-body clearing. *Cell.* 158:945–958.
- 42 Dodt HU, et al. 2007. Ultramicroscopy: three-dimensional visualization of neuronal networks in the whole mouse brain. *Nat Methods.* 4:331–336.
- 43 Ke MT, et al. 2016. Super-resolution mapping of neuronal circuitry with an index-optimized clearing agent. *Cell Rep.* 14:2718–2732.
- 44 Renier N, et al. 2014. iDISCO: a simple, rapid method to immunolabel large tissue samples for volume imaging. *Cell.* 159:896–910.
- 45 Unnersjö-Jess D, Scott L, Blom H, Brismar H. 2016. Super-resolution stimulated emission depletion imaging of slit diaphragm proteins in optically cleared kidney tissue. *Kidney Int.* 89:243–247.
- 46 Unnersjö-Jess D, et al. 2022. Three-dimensional super-resolved imaging of paraffin-embedded kidney samples. *Kidney360.* 3:446–454.
- 47 Kuppe C, et al. 2019. Novel parietal epithelial cell subpopulations contribute to focal segmental glomerulosclerosis and glomerular tip lesions. *Kidney Int.* 96:80–93.
- 48 Lazareth H, et al. 2019. The tetraspanin CD9 controls migration and proliferation of parietal epithelial cells and glomerular disease progression. *Nat Commun.* 10:3303.
- 49 Yamada H, et al. 2021. MAGI-2 orchestrates the localization of backbone proteins in the slit diaphragm of podocytes. *Kidney Int.* 99:382–395.
- 50 Susaki EA, et al. 2014. Whole-brain imaging with single-cell resolution using chemical cocktails and computational analysis. *Cell.* 157:726–739.
- 51 Hama H, et al. 2015. Scales: an optical clearing palette for biological imaging. *Nat Neurosci.* 18:1518–1529.
- 52 Shirata N, et al. 2017. Glomerulosclerosis induced by deficiency of membrane-associated guanylate kinase inverted 2 in kidney podocytes. *J Am Soc Nephrol.* 28:2654–2669.
- 53 Makino SI, et al. 2021. Impairment of proteasome function in podocytes leads to CKD. *J Am Soc Nephrol.* 32:597–613.
- 54 Asao R, et al. 2018. Rac1 in podocytes promotes glomerular repair and limits the formation of sclerosis. *Sci Rep.* 8:5061.